Research Square

Preprints are preliminary reports that have not undergone peer review.
They should not be considered conclusive, used to inform clinical practice,
or referenced by the media as validated information.

Black hole entropy production peaks before cosmic accretion and quasar light

Yang Su

yang.su@inrae.fr

École Normale Supérieure – PSL https://orcid.org/0000-0002-4717-9971

Research Article

Keywords: black hole physics, quasars: supermassive black holes, galaxies: active, galaxies: evolution, methods: numerical

Posted Date: November 25th, 2026

DOI: https://doi.org/10.21203/rs.3.rs-11859386/v1

License: This work is licensed under a Creative Commons Attribution 4.0 International License.
Read Full License

Additional Declarations: The authors declare no competing interests.

Abstract

Gas accretion increases black hole horizon entropy at a rate proportional to black hole mass times mass growth. We ask when this rate peaked relative to cosmic gas accretion and quasar light. We integrate the Trinity black hole population over one million to ten billion solar masses and locate the three peaks within each posterior history. Mass-weighted gas growth peaks at redshift 2.4, a median 0.60 Gyr before unweighted gas accretion (central 95% posterior interval 0.45–0.77 Gyr earlier) and 0.80 Gyr before bolometric quasar light (0.55–1.08 Gyr earlier). All 999 retained histories give this ordering of weighted growth relative to each comparator. The earlier maximum relative to gas accretion contrasts with the later maximum found in a recent characteristic-mass entropy ledger. In the 27 CAMELS-IllustrisTNG simulations of the cosmic variance (CV) set, the pooled growth peak precedes the light peak by 0.90 Gyr. Omitting the largest accretion contribution at the peak snapshot reduces the lead to 0.07 Gyr. Resampling complete boxes gives a 95% interval from 1.02 Gyr earlier to 0.20 Gyr later. With a Gaussian smoothing width of 0.5 Gyr, growth leads light by 0.16 Gyr in CAMELS (bootstrap interval 0.04–0.34 Gyr earlier) and by a median 0.73 Gyr in Trinity. Both smoothed histories favor earlier mass-weighted growth, while the inferred separation depends on the population model.

1 Introduction

A black hole that gains a given amount of mass adds more horizon area if it is already massive. This follows directly from the area law for a nonrotating hole (Bekenstein 1973; Hawking 1975). Entropy inventories therefore give exceptional weight to the most massive black holes (Egan & Lineweaver 2010). Timing introduces a further requirement. A massive remnant contributes to the inventory throughout its lifetime, whereas its contribution to accretion-driven entropy growth depends on whether it is still being fed.

The integrated light of active galactic nuclei provides a constraint on the mass accumulated by accretion (Sołtan 1982). Luminosity functions also encode the decline of the most luminous active nuclei, and demographic models infer that the most massive black holes assembled much of their mass early while less massive ones grew later (Merloni 2004; Hasinger, Miyaji & Schmidt 2005; Merloni & Heinz 2008; Shankar et al. 2009; Ueda et al. 2014). Surveys of the joint mass and accretion-rate distributions show why the distinction matters: selection in luminosity changes the active mass distribution that enters an observed sample (Kelly & Shen 2013; Schulze et al. 2015).

Izaurieta et al. (2026) constructed an entropy ledger in which the horizon term is the cosmic accretion history multiplied by a characteristic mass, the accumulated black hole mass density divided by a fixed effective number density. Because that mass grows monotonically, their fiducial entropy production rate peaks at $z \approx 1.2$, later than the accretion peak near $z \approx 2$. The approximation assigns late accretion to the typical mass of all black holes, whereas luminosity-dependent evolution implies that late accretion is dominated by less massive black holes. We test whether resolving this distribution changes the ordering of the entropy and gas-accretion maxima. Trinity, an empirical model connecting halos, galaxies, and

black holes, predicts a declining contribution from massive accretors over part of cosmic time (Zhang et al. 2023, 2024) and resolves the black hole mass distribution at every epoch. We ask whether the two peaks can be distinguished after carrying uncertainty in the entire population history into the comparison. The target is the gas-accretion channel in a fixed comoving volume.

Hydrodynamical calculations have already traced the buildup of cosmic entropy (Zhao et al. 2012), and Illustris has resolved the accretion history by black hole mass (Sijacki et al. 2015). The quantity at issue here is the paired time difference between two maxima within the same population. We apply the same mass limits, sign convention, and temporal-resolution tests to a fitted demographic history and to a hydrodynamical simulation that evolves individual black holes. This design separates agreement about which channel peaks first from agreement about the numerical separation.

2 Methods

2.1 Three population histories

Let n denote the comoving abundance measure over black hole mass M and host properties; brackets denote conditional averages at fixed mass and host. We evaluate the following quantities over the same mass interval at every epoch.

$j = \int \langle L \rangle \, dn$, $W = \int M \langle L \rangle \, dn$, $G = \int M \langle dM/dt \rangle_{gas} \, dn$. (1)

Here L is bolometric radiative luminosity and the mass derivative is the gravitational mass gained through gas accretion. For a Schwarzschild black hole, $S = 4\pi k_B G_N M^2/(\hbar c)$, with Newton's constant denoted by G_N. The comoving entropy growth rate is therefore $8\pi k_B G_N G/(\hbar c)$ in consistent units. We compare the peaks of G and j. W is a diagnostic with the same timing as G when emitted energy per unit mass gained is constant. Trinity allows the relation between bolometric light and accretion to vary with accretion state. All three quantities are estimated independently of any assumption about the total cosmic entropy.

The Schwarzschild form is an accounting choice. For a Kerr black hole of dimensionless spin a, $S = 2\pi k_B G_N M^2[1 + (1 - a^2)^{1/2}]/(\hbar c)$. For a spin distribution of accreting black holes that is constant in time, the spin factor rescales the entropy rate without moving its maximum.

2.2 Continuous integration within the mass bins

We use the public Trinity release at commit 89de894d1a6b1d91a4e2cf26092dec4b4ad1678b, its Bolshoi-Planck halo cache, and the parameter vectors in stats/down_sampled_chain.dat. At each halo mass and redshift, the code supplies a median $\log_{10}$ black hole mass m, a scatter s in dex, a black hole occupation fraction, a mean gas-growth rate, and an Eddington-ratio distribution. The scatter combines dispersion in stellar mass and in the black hole–bulge relation in quadrature. In the released model the parameter controlling residual mass dependence of the Eddington ratio is fixed at unity (rho_bh = 1).

Thus the mean Eddington ratio at given halo mass is independent of the residual black hole mass, and the conditional mean luminosity is proportional to M.

Masses in the integration are expressed in solar masses. If $X = \log_{10} M$ follows a Gaussian with mean m and variance s^2, the unnormalized kth moment in the interval $a < X < b$ is given by Eq. (2). Φ is the standard normal cumulative distribution function and $u = k \ln 10$.

$T_k = \exp(um + u^2 s^2/2) \times \{\Phi[(b - m - us^2)/s] - \Phi[(a - m - us^2)/s]\}$. (2)

The implementation calls Trinity's halo and black hole growth routines and integrates its radiative Eddington-ratio distribution in log space, including the duty and occupation factors used by its luminosity function. In a halo population with radiative coefficient A, j receives A T_1 and W receives A T_2. For G we normalize the conditional gas-growth rate to the released mean rate for occupied hosts, then multiply T_2 by the mean growth divided by the mean black hole mass and by the occupied halo density. This allocation gives mean gas growth proportional to M at fixed halo. The ratio W/j directly recovers the luminosity-weighted mass inside a decade without assigning a single mass to every source. As a numerical check, we also sum the original Trinity two-dimensional luminosity-function grid, with fractional coverage at mass boundaries, for its released best-fit parameters. For the unweighted gas-accretion history we use the same conditional rate and mass limits, replacing T_2 with T_1. We locate its peak separately in each draw and pair it with the growth and light peaks from that draw.

2.3 Correlated histories and peak inference

The release documentation describes 1,024 draws; the pinned file contains 1,000 distinct numeric rows. All were evaluated. One row triggered a negative-accretion validity flag during the early model evolution. The primary sample comprises the remaining 999 rows; a sensitivity calculation restores the flagged row. Each draw provides one coherent trajectory through 126 snapshots at $0 \le z \le 5.932$. We integrate over one million to ten billion solar masses. A flat matter-plus-Λ expansion with $H_0 = 67.4$ km s^{-1} Mpc^{-1} and $\Omega_m = 0.315$ converts redshift to cosmic age (Planck Collaboration 2020).

Within a draw, we locate each history's global grid maximum and interpolate the logarithm of its rate with a quadratic through that point and its two temporal neighbors. The vertex is restricted to the bracketing interval. Subtracting the age of the light maximum from the growth maximum gives Δt; negative values indicate earlier growth. Quantiles are taken across paired differences. We additionally report the discrete-grid result, the effect of extending or truncating the mass interval, and the contrast with replacing the continuous mass inside each decade by its geometric midpoint. To test the allocation of growth, we also set the conditional gas-growth rate proportional to M^p with p = 0 or 2, conserving the mean rate within each halo over its full mass distribution. The light history is held at its fiducial form in these tests.

2.4 Independent particle-level test with CAMELS

We use all 27 simulations of the cosmic variance (CV) set of the CAMELS-IllustrisTNG suite (Villaescusa-Navarro et al. 2021, 2023), which use the IllustrisTNG galaxy formation model (Weinberger et al. 2017; Pillepich et al. 2018). The boxes share physical parameters and differ in initial phases. Each has a side length of 25 comoving Mpc/h, with h = 0.6711 and Ω_m = 0.30. The 34 available snapshots span z = 0–5.994. Their black hole particles supply subgrid mass (BH_Mass) and instantaneous gas inflow rate (BH_Mdot). We convert masses by 10^{10}/h solar masses and rates by 10/0.978 solar masses per year per code unit. The primary mass cuts retain 955,897 particle–snapshot records in a total comoving volume of 1.396 million cubic megaparsecs. Repeated observations of a particle are part of its trajectory. The lower mass limit lies just below the seed mass of 8×10^5 h^{-1} ($\approx 1.19 \times 10^6$) solar masses, so newly seeded black holes enter the sample; because of the M^2 weighting, records below 2×10^6 solar masses supply less than 0.02% of the integrated growth.

For inflow rate D and radiative efficiency ε = 0.2, we sum (1 − ε)MD per volume for growth. For quasar light we use $L = \varepsilon D c^2 \min(1, 10\lambda)$, with $\lambda = \varepsilon D c^2 / L_{Edd}$ and $L_{Edd} = 1.26 \times 10^{38}$ erg s^{-1} per solar mass times M. This post-processing gives quadratic radiative output below λ = 0.1 and linear output above it (Churazov et al. 2005; Habouzit et al. 2019). We also test linear output throughout. The luminosities are derived from the simulation inflows. We take the peak of the mean rate across boxes and resample 27 complete boxes with replacement 5,000 times, using the same box indices for both curves and at every epoch. These percentile intervals quantify finite-volume variation at fixed subgrid physics.

We use the same three-point peak interpolator as for Trinity. For cadence matching, we interpolate each Trinity log-rate in cosmic time to the CAMELS snapshots, using the nearest endpoint for the single snapshot just beyond the Trinity range. A normalized Gaussian kernel in cosmic time, weighted by the local snapshot spacing, supplies sensitivity tests at standard deviations of 0.3, 0.5 and 1.0 Gyr. Smoothing defines the peak of sustained activity on a specified timescale. The unsmoothed maximum instead retains brief bright episodes. We use the same age conversion as in Section 2.3 for comparison and repeat the raw test with the simulation cosmology.

3 Results

3.1 The paired peak difference

The median peak ages are 3.50 Gyr for quasar light and 2.72 Gyr for mass-weighted gas growth. Their separate central 95% intervals are 3.29–3.73 and 2.48–2.97 Gyr. At the median ages the corresponding redshifts are approximately 1.86 and 2.41. The paired median Δt is − 0.799 Gyr, with a central 68% interval of − 0.939 to − 0.666 Gyr and a central 95% interval of − 1.078 to − 0.554 Gyr. Every retained draw places growth first. At the light maximum the growth curve still retains a median 86.9% of its own maximum (95% interval 77.5–93.8%). Figures 1 and 2 distinguish overlap of the two broad histories from uncertainty in their peak separation. Unweighted gas accretion peaks at a median age of 3.29 Gyr (95% interval 3.09–3.56 Gyr). Mass-weighted growth precedes it in all 999 draws, by a median 0.60 Gyr (95%

interval 0.45–0.77 Gyr earlier). The paired difference between unweighted gas and light peaks is − 0.18 Gyr (95% interval − 0.44 to + 0.01 Gyr).

Taking the tabulated maxima without interpolation gives Δt = − 0.816 Gyr (95% interval − 1.056 to − 0.544). Restoring the flagged draw gives − 0.800 Gyr. Splitting the retained file order into four approximately equal groups gives median lags between − 0.816 and − 0.787 Gyr. These checks address timing resolution, the validity filter, and finite-sample stability.

3.2 Resolving masses and recovering gas growth

Using mass-weighted light gives Δt = − 0.482 Gyr (95% interval − 0.713 to − 0.279). Geometric decade midpoints give − 0.426 Gyr (− 0.647 to − 0.244). Within paired draws, resolving the luminosity-weighted mass changes the peak age by a median − 0.041 Gyr; replacing mass-weighted light with mass-weighted gas growth changes it by another − 0.284 Gyr. For the best fit, numerical summation over Trinity's native mass–luminosity grid agrees with the continuous reconstruction of both radiative moments to within 0.0011 dex throughout the sampled history. This validates the radiative integration against the upstream code. The gas-growth moment additionally uses the specified allocation of the mean accretion rate.

The ratio $W/(c^2G)$ is a population mean of radiated energy per unit gas mass gained, weighted by black hole mass times gas growth. Its posterior median is 0.065 at $z \approx 4–5$ (68% interval 0.055–0.080), 0.084 at $z \approx 1.7$ (0.066–0.110), and 0.034 at $z = 0$ (0.024–0.045). Within draws, the ratio at the light peak exceeds its value at the mass-weighted growth peak by a median 11% (95% interval 2–32%). Mass-weighted light peaks a median 0.48 Gyr before total light. Mass-weighted growth peaks a median 0.28 Gyr before mass-weighted light. These paired differences describe how the peak shifts under successive changes of weight.

At the gas-growth peak, objects between one and ten billion solar masses provide a median 17.3% of the light (95% interval 13.2–21.8%) and 63.5% of mass-weighted gas growth (58.0–68.4%). Restricting both integrals to black holes below one billion solar masses reduces the median lead to 0.387 Gyr (0.164–0.624). Extending the upper bound to 100 billion solar masses increases it to 0.859 Gyr (0.618–1.166). The largest decade amplifies an ordering already present among less massive accretors.

3.3 Dependence on the accretion allocation

Allocating the same mean halo-hosted gas growth independently of residual black hole mass ($p = 0$) gives a median Δt of − 0.798 Gyr (95% interval − 1.106 to − 0.539); assigning growth proportional to mass squared gives − 0.703 Gyr (− 0.969 to − 0.481). Within this family of allocations, the ordering is therefore insensitive to how gas growth is shared among black holes in the same halo. Appendix A shows that the black hole mass scale of an optically selected quasar sample depends on the virial calibration at a level comparable to the evolution between the two epochs.

3.4 An independent hydrodynamical population

The pooled CAMELS growth and light peaks occur at ages 2.09 and 3.00 Gyr, respectively (Fig. 5), a difference of − 0.901 Gyr. This growth maximum is a single-snapshot feature. At z = 3.0 the pooled growth rate is 1.43 times its value at the following snapshot (z = 2.81) and at least 1.12 times every later snapshot; between z = 2.63 and 2.15 it stays at 0.81–0.90 of the maximum. One black hole in box 7, with a mass of 1.48×10^9 solar masses and an accretion rate of 3.1 solar masses per year, supplies 13.2% of the pooled growth at that snapshot, and the five largest records supply 36%. Removing that single record moves the pooled growth maximum to 2.92 Gyr (z ≈ 2.2) and reduces the difference to − 0.075 Gyr; removing the entire snapshot gives the same result.

The bootstrap median is − 0.579 Gyr; the central 95% percentile interval is [− 1.020, + 0.203] Gyr and 81.3% of replicates place growth first. The two modes are associated with the inclusion of box 7. Replicates that contain it (62.8%) give a median − 0.823 Gyr, and the others give − 0.065 Gyr. Omitting one box at a time gives differences from − 0.926 to − 0.055 Gyr. Using the simulation cosmology gives − 0.926 Gyr for the pooled difference. A linear luminosity conversion gives − 0.917 Gyr, again with a bootstrap interval crossing zero.

On matched unsmoothed snapshots, Trinity gives a median − 0.787 Gyr (95% interval − 1.078 to − 0.550). At 0.5 Gyr smoothing, the pooled CAMELS difference is − 0.161 Gyr (bootstrap interval − 0.335 to − 0.037), whereas the Trinity median is − 0.725 Gyr (posterior interval − 0.981 to − 0.514). CAMELS pooled differences for widths of 0.3 and 1.0 Gyr are − 0.110 and − 0.217 Gyr. The near-agreement of the unsmoothed estimates (− 0.79 and − 0.90 Gyr) depends on temporal resolution. After smoothing, the CAMELS lead falls to 0.1–0.2 Gyr while the Trinity lead stays above 0.7 Gyr (Fig. 6). At the CAMELS growth-peak snapshot, only three selected black holes exceed one billion solar masses. Together they supply 13.3% of growth, compared with a median 63.5% at the Trinity growth peak. These figures show the different population weights of the two models and the leverage of rare episodes in CAMELS.

4 Discussion

The result separates two questions that lead to different numerical answers. If every unit of emitted energy traces the same gain in black hole mass, the inferred lead is about half a billion years. When the model’s gas supply is used directly, the lead approaches eight hundred million years, because the fitted ratio of radiated energy to mass gained is highest near the quasar peak (Section 3.2). Radiative efficiency and the Eddington-ratio distribution connect these histories. The timing of horizon entropy growth therefore depends both on the luminosity-weighted mass and on which black holes gain mass with weak radiative output. An inventory dominated by massive remnants today is compatible with an earlier maximum in the rate at which their horizons grew.

The characteristic-mass ledger of Izaurieta et al. (2026) places its horizon-growth maximum after the gas-accretion maximum. In Trinity the ordering reverses over the selected mass range. Weighting the same gas-accretion history by the masses of the accreting black holes moves its maximum earlier by a median 0.60 Gyr. This comparison uses gas growth on both sides and is independent of the choice to

use quasar light as an observational reference. The two studies use different underlying accretion histories; the comparison above isolates the effect of mass weighting within one history. Our calculation applies to gas accretion in a fixed comoving volume.

The posterior intervals propagate the covariance of mass assembly, radiative activity, and redshift evolution allowed by the published Trinity fit. In this fit, accretion builds horizon entropy fastest well before the maximum in quasar light, and about a third of that lead comes from the fitted evolution of radiative output per unit mass gained.

In the CAMELS-IllustrisTNG simulations, the unsmoothed pooled lead falls from 0.90 to 0.07 Gyr when one particle record is omitted, the box-bootstrap interval spans both orderings, and with 0.5 Gyr smoothing growth leads by 0.16 Gyr. The ordering persists after temporal averaging in both models, while the size of the lead differs between them. A volume of 25 h^{-1} comoving Mpc on a side contains few black holes above 10^9 solar masses, the mass range that supplies most of the mass-weighted growth in Trinity.

Declarations

Acknowledgments

This work uses the public CAMELS simulations and Trinity model, the Sloan Digital Sky Survey, and the VizieR catalog service.

Data availability

The data and code used in this study are available on Figshare at https://doi.org/10.6084/m9.figshare.35107012. The archive contains the Trinity parameter vectors, draw-by-epoch mass moments, peak summaries, the best-fit native-grid check, and the selected SDSS catalog columns (VizieR J/ApJS/194/45). For the CAMELS comparison, it contains the selected particle masses and inflow rates, per-box histories, bootstrap differences, and matched-cadence Trinity draws. The executed notebook reproduces the reported distributions, figures, and diagnostics. A second notebook rebuilds the moment extraction from the pinned public Trinity source, and Python helpers reproduce the CAMELS extract from the public IllustrisTNG CV particle snapshots hosted by the Flatiron Institute.

References

1. Bekenstein JD (1973) Black Holes and Entropy. Phys Rev D 7:2333. 10.1103/PhysRevD.7.2333
2. Churazov E, Sazonov S, Sunyaev R, Forman W, Jones C, Böhringer H (2005) Supermassive black holes in elliptical galaxies: switching from very bright to very dim. MNRAS 363:L91. 10.1111/j.1745-3933.2005.00093.x

3. Egan CA, Lineweaver CH (2010) A Larger Estimate of the Entropy of the Universe. ApJ 710:1825. 10.1088/0004-637X/710/2/1825
4. Habouzit M et al (2019) Linking galaxy structural properties and star formation activity to black hole activity with IllustrisTNG. MNRAS 484:4413. 10.1093/mnras/stz102
5. Hasinger G, Miyaji T, Schmidt M (2005) Luminosity-dependent evolution of soft X-ray selected AGN. New Chandra and XMM-Newton surveys. A&A, 441, 417. 10.1051/0004-6361:20042134
6. Hawking SW (1975) Particle creation by black holes. Commun Math Phys 43:199. 10.1007/BF02345020
7. Izaurieta F, Quinzacara C, Valdivia O (2026) How greedy is the Universe? An entropy ledger and a causal envelope for early black hole growth. Preprint, arXiv:2608.00297
8. Kelly BC, Shen Y (2013) The demographics of broad-line quasars in the mass–luminosity plane. II. Black hole mass and Eddington ratio functions. ApJ 764:45. 10.1088/0004-637X/764/1/45
9. Merloni A (2004) The anti-hierarchical growth of supermassive black holes. MNRAS 353:1035. 10.1111/j.1365-2966.2004.08147.x
10. Merloni A, Heinz S (2008) A synthesis model for AGN evolution: supermassive black holes growth and feedback modes. MNRAS 388:1011. 10.1111/j.1365-2966.2008.13472.x
11. Pillepich A et al (2018) Simulating galaxy formation with the IllustrisTNG model. MNRAS 473:4077. 10.1093/mnras/stx2656
12. Planck Collaboration, (2020) Planck 2018 results. VI. Cosmological parameters. A&A, 641, A6. 10.1051/0004-6361/201833910
13. Schulze A et al (2015) The cosmic growth of the active black hole population at $1 < z < 2$ in zCOSMOS, VVDS and SDSS. MNRAS, 447, 2085. 10.1093/mnras/stu2549
14. Shankar F, Weinberg DH, Miralda-Escudé J (2009) Self-consistent models of the AGN and black hole populations: duty cycles, accretion rates, and the mean radiative efficiency. ApJ 690:20. 10.1088/0004-637X/690/1/20
15. Shen Y et al (2011) A catalog of quasar properties from Sloan Digital Sky Survey Data Release 7. ApJS 194:45. 10.1088/0067-0049/194/2/45
16. Sijacki D et al (2015) The Illustris simulation: the evolving population of black holes across cosmic time. MNRAS 452:575. 10.1093/mnras/stv1340
17. Sołtan A (1982) Masses of quasars. MNRAS 200:115. 10.1093/mnras/200.1.115
18. Ueda Y, Akiyama M, Hasinger G, Miyaji T, Watson MG (2014) Toward the standard population synthesis model of the X-ray background. ApJ 786:104. 10.1088/0004-637X/786/2/104
19. Vestergaard M, Osmer PS (2009) Mass functions of the active black holes in distant quasars. ApJ 699:800. 10.1088/0004-637X/699/1/800
20. Villaescusa-Navarro F et al (2021) The CAMELS Project: Cosmology and Astrophysics with Machine-learning Simulations. ApJ 915:71. 10.3847/1538-4357/abf7ba

21. Villaescusa-Navarro F et al (2023) The CAMELS Project: Public Data Release. ApJS 265:54. 10.3847/1538-4365/acbf47
22. Weinberger R et al (2017) Simulating galaxy formation with black hole driven thermal and kinetic feedback. MNRAS 465:3291. 10.1093/mnras/stw2944
23. Weinberger R et al (2018) Supermassive black holes and their feedback effects in the IllustrisTNG simulation. MNRAS 479:4056. 10.1093/mnras/sty1733
24. Zhang H et al (2023) Trinity I: self-consistently modelling the dark matter halo–galaxy–supermassive black hole connection from z = 0–10. MNRAS 518:2123. 10.1093/mnras/stac2633
25. Zhang H et al (2024) Trinity III: quasar luminosity functions decomposed by halo, galaxy, and black hole masses as well as Eddington ratios from z = 0–10. MNRAS 529:2777. 10.1093/mnras/stae655
26. Zhao X, Li Y, Zhu Q, Fox D (2012) The co-evolution of cosmic entropy and structures in the universe. arXiv:1211.1677.

Figures

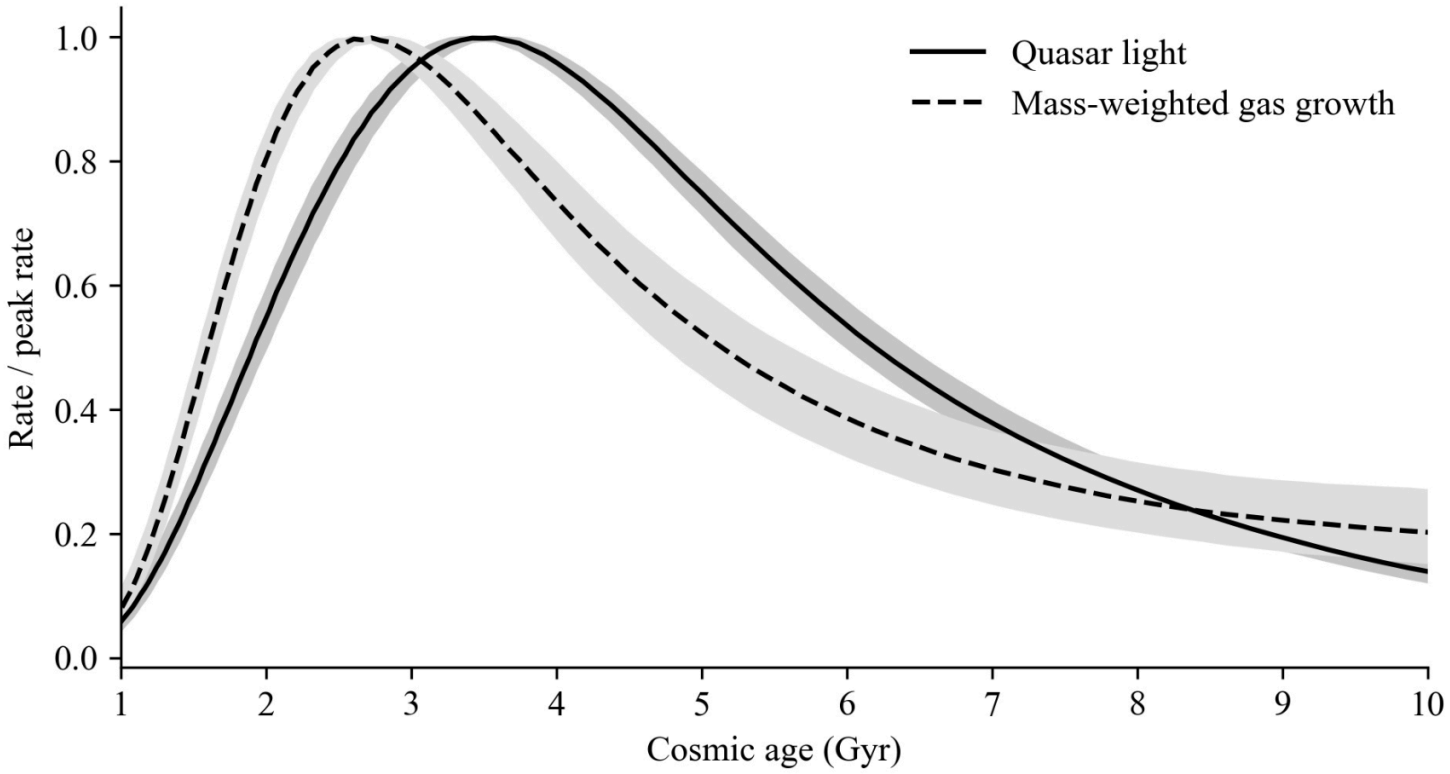

Figure 1

Quasar luminosity density and mass-weighted gas growth versus cosmic age. Each draw is divided by its own peak rate before summarizing. Lines give posterior medians and shading spans the 16th–84th percentiles at each epoch. The time axis shows the interval around both peaks.

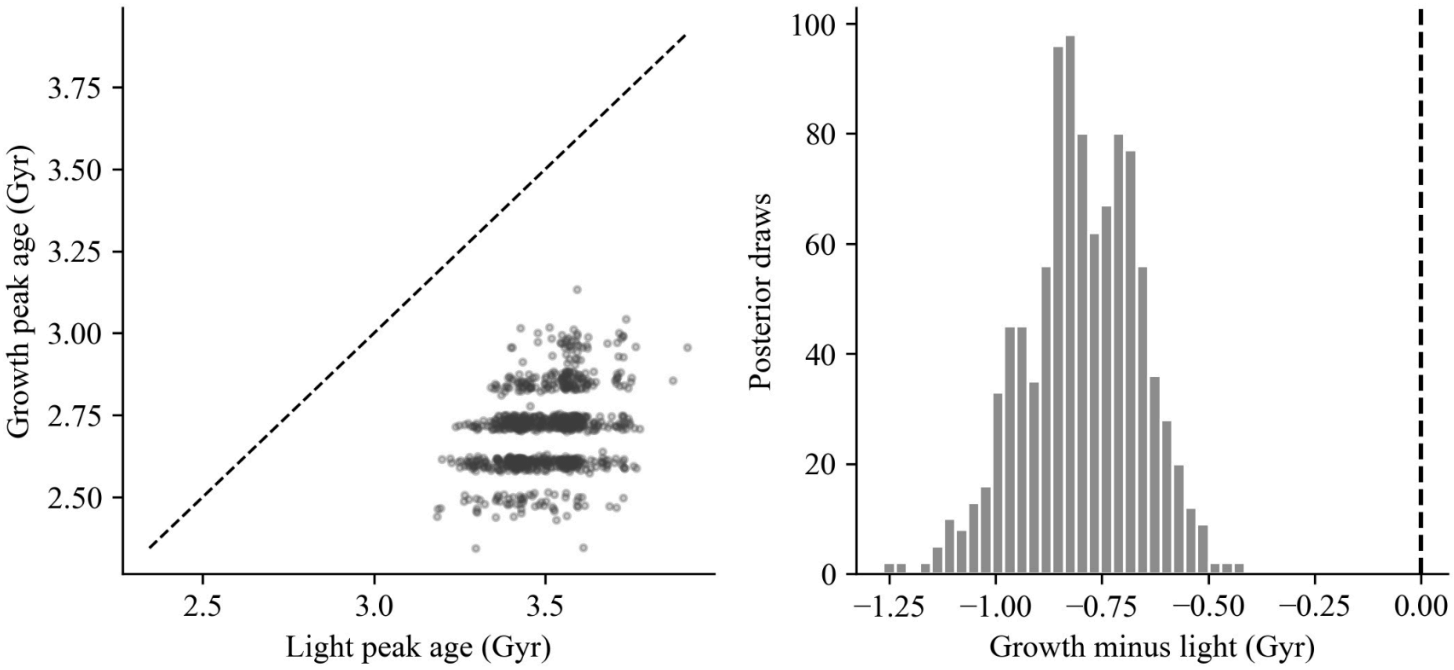

Figure 2

Left: peak ages from matched parameter draws; the dashed line indicates simultaneous peaks. Right: distribution of the paired difference. Both panels use the same 999 draws.

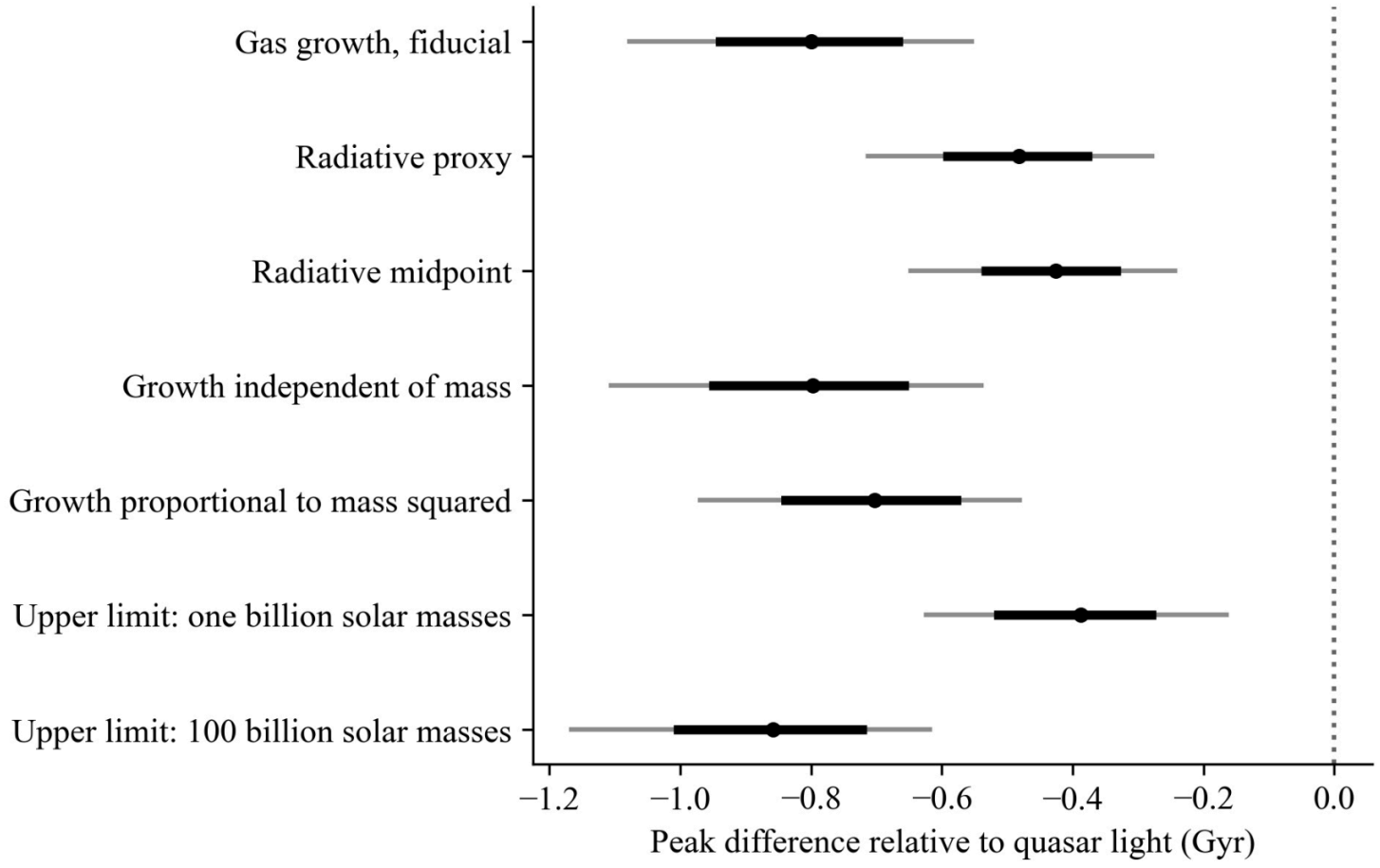

Figure 3

Median paired time differences, with central 68% (thick) and 95% (thin) intervals. The upper-mass-limit tests use the same truncated population for growth and light. The alternative growth prescriptions retain the fiducial light history.

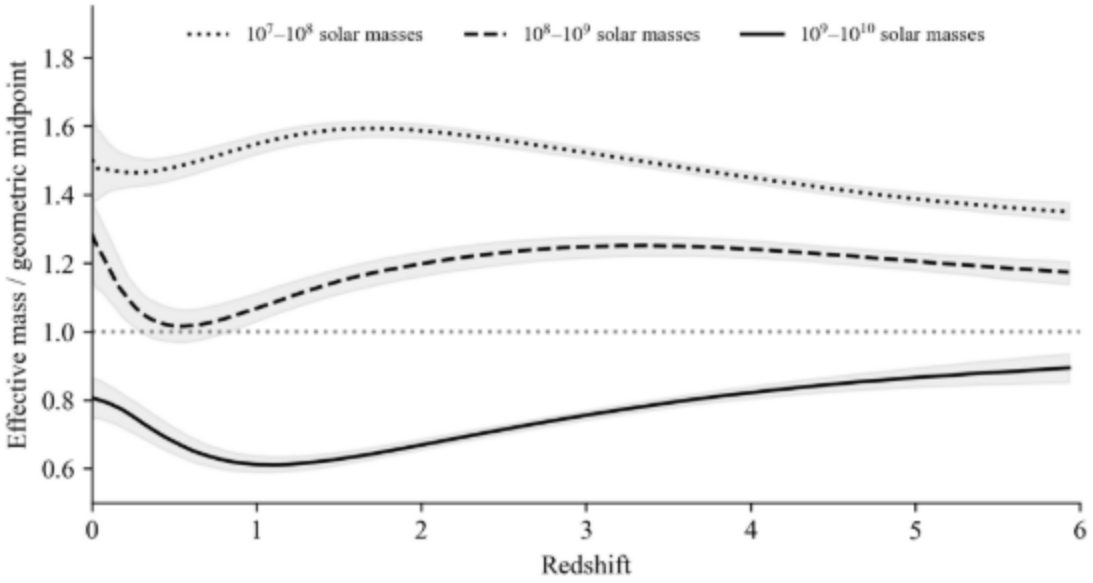

Figure 4

Recovered luminosity-weighted mass in three decades, divided by the geometric midpoint of each decade. Lines and shading give medians and central 68% intervals. Evolution of this ratio changes the entropy proxy even at fixed integrated light in a mass bin.

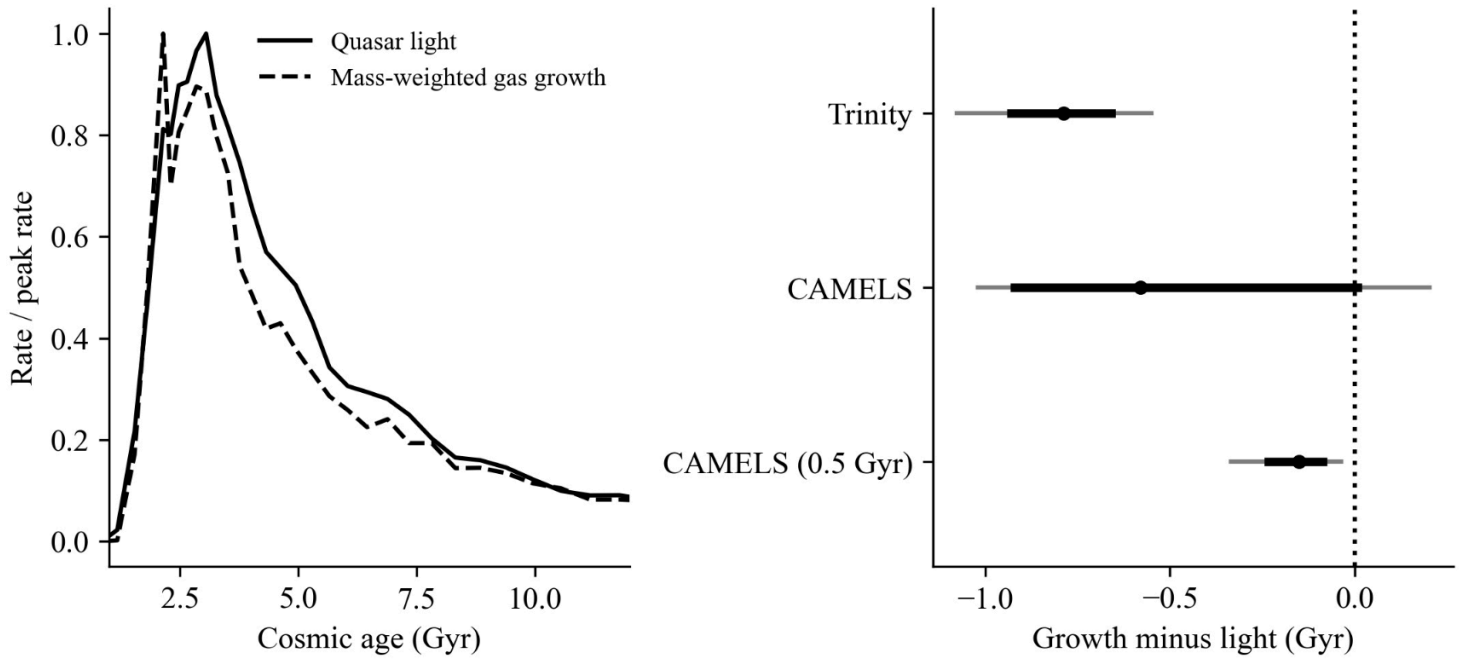

Figure 5

Left: unsmoothed CAMELS histories summed over all boxes, each normalized to its own maximum. Right: medians, central 68% intervals, and central 95% intervals. Trinity uses matched snapshot times and joint posterior draws. CAMELS uses complete-box bootstrap samples; the third row applies 0.5 Gyr smoothing. The narrow growth maximum near 2.1 Gyr in the left panel changes rank when the largest particle record at that snapshot is omitted (Section 3.4).

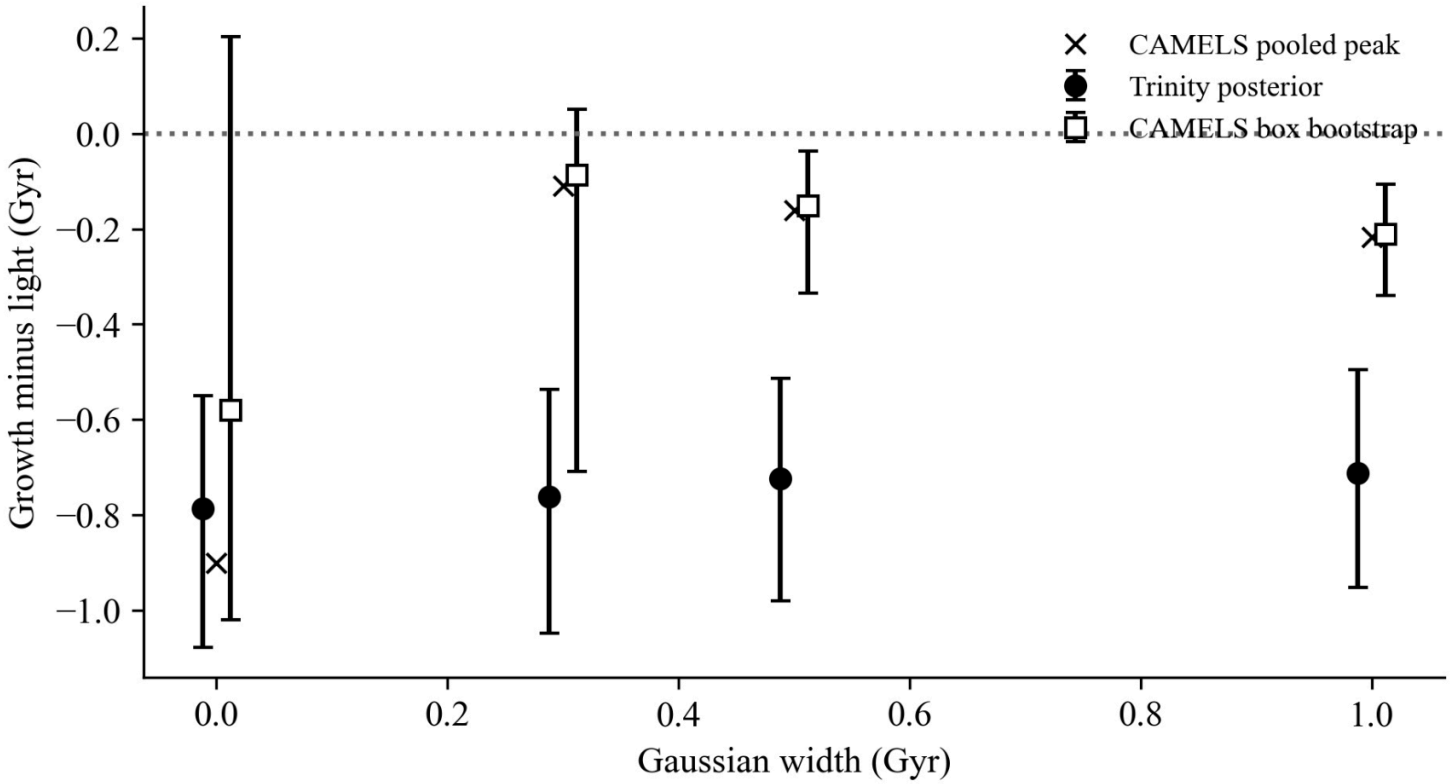

Figure 6

Peak differences at matched temporal resolution. Filled and open symbols show the Trinity posterior and CAMELS bootstrap medians, respectively, with central 95% intervals. Crosses are the CAMELS pooled estimates. Zero width denotes unsmoothed sampling; the two sets of interval markers are offset horizontally for visibility.

Supplementary Files

This is a list of supplementary files associated with this preprint. Click to download.

- AppendixA.docx